Journal of the Brazilian Society of Mechanical Sciences and Engineering (2021) 43:328
https://doi.org/10.1007/s40430-021-03037-x

TECHNICAL PAPER

An approximate analytic solution of uniform laminar flow in a circular open channel

Kenan Kaya[1] · **Oktay Özcan**[1]

Received: 11 November 2020 / Accepted: 15 May 2021 / Published online: 3 June 2021

Abstract
An approximate analytic solution of the Navier–Stokes equations for laminar flow in a circular open channel is presented. The solution is valid for the case of incompressible steady uniform flow in a low-filled channel. (The depth ratio, which is flow depth divided by channel radius, is smaller than one.) The solution is compared with a recently reported exact theoretical solution and found to be in reasonably good agreement. Expressions for variation of the correction factors for momentum and kinetic energy fluxes with flow depth are presented. A correlation between the momentum and kinetic energy flux correction factors is proposed and compared with data reported in the literature.

Keywords Free-surface flow · Navier–Stokes equations · Velocity distribution · Momentum flux correction factor · Kinetic energy flux correction factor

List of symbols

C_1, C_2	Integration constants
Fr	Froude number
g	Gravitational acceleration
h	Flow depth
P	Pressure
r	Radial coordinate
r_s	Distance from the pipe center to a point on the free surface
R	Pipe radius
Re	Reynolds number
T_0	Normalized wall shear stress
U	Normalized streamwise velocity
U_b	Normalized bulk velocity
U_o	Dimensionless centerline surface velocity
V_b	Bulk velocity
V_x, V_r, V_θ	Velocity components in cylindrical coordinate system
x, y, z	Spatial coordinates in the Cartesian system
y_s	Vertical distance from a point on the pipe wall to the free surface
α	Kinetic energy flux correction factor
β	Momentum flux correction factor
μ	Dynamic viscosity
φ	Maximum value of the azimuthal coordinate corresponding to a particular flow depth
$\varnothing$	Pipe inclination angle
ρ	Density
θ	Azimuthal coordinate

1 Introduction

Analytical solutions of the Navier–Stokes equations are rare due to their nonlinearity. An extensive review of exact solutions was presented by Berker [1]. A more recent review of unsteady flow solutions is reported by Wang [2]. Berker [3] and Rajagopal [4] report existence of an infinite set of exact solutions for a certain flow occurring in an orthogonal rheometer. Terrill and Colgan [5] present some axisymmetric solutions for permeable boundaries with a circular cross section that vary in the axial direction.

An exact solution for pressure driven fully developed laminar pipe flow exists, that is, the well-known Hagen-Poiseuille solution [6]. However, finding exact solutions to flows with more complex geometries, including those in ducts of arbitrary cross section and in partially full conduits involving a free surface, are challenging. Therefore, numerical or semi-analytical approaches were proposed

Technical Editor: Monica Carvalho.

✉ Kenan Kaya
kenankaya@aydin.edu.tr

[1] Department of Mechanical Engineering, Istanbul Aydin University, Kucukcekmece, 34295 Istanbul, Turkey

previously. O'Brien [7] adopted a finite-difference approximation to solve the momentum equation numerically and obtained velocity profiles for flow in ducts of arbitrary cross section, whereas McKerrell [8] conducted numerical calculations to solve the same problem using the global element method. For the same purpose, Duck [9] used conformal mapping and Fourier series expansion. Mazumdar and Dubey [10] obtained an approximate analytical solution to the same problem by assuming a function for isovelocity contours and then solving the momentum equation. Recent analytical solutions for Jeffery-Hamel flow are reported by Sari et al. [11] and Kezzar and Sari [12] by application of the Adomian and generalized decomposition methods.

None of the studies discussed above consider flow problems with a free surface, in which case flow depth is introduced as an additional variable determining the velocity profile. Free-surface flows (also known as open-channel flows) are encountered in natural systems, such as rivers, as well as in artificial channels, i.e., dams, culverts, and subsurface water drains. There are also industrial applications involving free-surface flows, such as solid transport, waste removal and metal casting. In the present study, we are interested in obtaining approximate solutions to partially filled laminar flow in circular pipes, for which Guo and Meroney [13] report a lack of theoretical and experimental studies and present a survey of previous work on the subject. Using bipolar coordinates and the Fourier transform, Guo and Meroney [13] solve the laminar incompressible flow Navier–Stokes equations for an arbitrary flow depth smaller or larger than the channel radius. Fullard and Wake [14] use the solution of Guo and Meroney [13] (whose integrals must be evaluated numerically) to obtain an analytical series solution (which also requires numerical evaluation).

The primary aim of the present study is to describe an approximate solution of the laminar velocity field for the case of low-filled circular channels (the depth ratio, i.e., flow depth divided by channel radius, is smaller than one), which has a simple analytic form suitable for easy evaluation, in contrast to the solutions presented previously in the literature. For this purpose, some approximations are employed to obtain a pure analytical solution of the steady incompressible Navier–Stokes equations in cylindrical coordinates. The accuracy of the assumptions made in the derivation of the approximate solution is assessed by comparing the approximate solution results with those of the exact solution of Guo and Meroney [13]. A secondary aim is to calculate some integral flow parameters (correction factors for momentum and kinetic energy fluxes) which are not reported in the literature for this flow. Variation of these parameters with depth ratio is currently unknown. Such analytic solutions for open-channel flows, which do not require rigorous calculations, have not been reported in the literature.

In the next section, the approximate solution procedure is described, and in the results section, the solution is compared with that of Guo and Meroney [13] in terms of cross-sectional velocity distribution, friction coefficient and some integral parameters (bulk velocity, correction factors for momentum and kinetic energy fluxes). Curve fitting is applied to the exact solution of Guo and Meroney [13] to obtain variation of the parameters mentioned above, with the depth ratio, which is not presented in their original work.

2 Solution

Side and sectional views of the flow geometry are shown in Fig. 1 where R is the pipe radius, h is the uniform flow depth and $\varnothing$ is the inclination angle of the channel. Direction of the gravitational acceleration g is also shown. The (x, y, z) Cartesian and (x, r, θ) cylindrical coordinate systems have origins on the x symmetry axis of the circular channel. Guo and Meroney

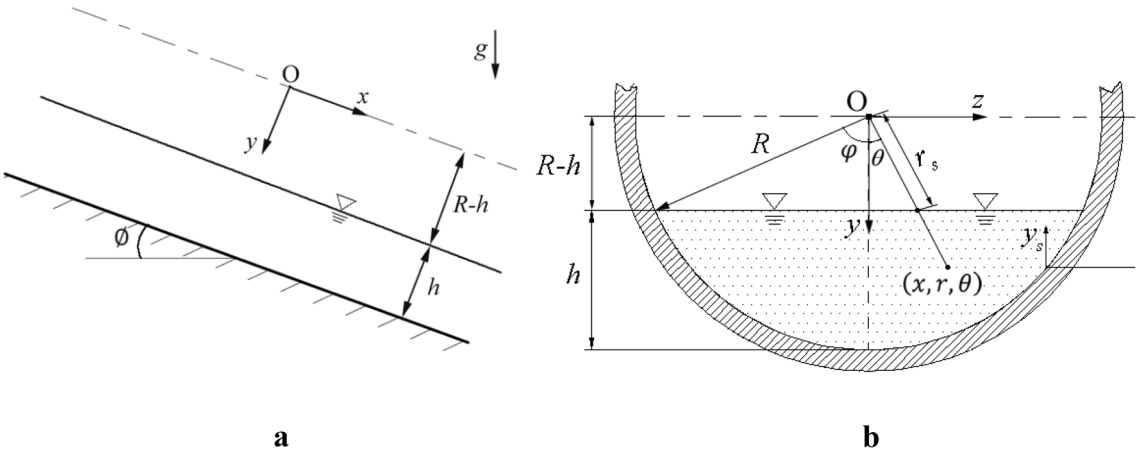

Fig. 1 Flow geometry and coordinate system: **a** side view and **b** cross-sectional view

[13] employ a bipolar coordinate system whose origin is located on the free surface and the plane of flow symmetry ($z=0$). It is assumed that Bond number of the flow considered is high enough, so that surface tension effects are negligible allowing a planar free surface, as it was also the case in [13].

The general momentum equation in the streamwise direction x for steady, laminar, incompressible flow can be written in cylindrical coordinates as follows [6]:

$$\rho\left(V_r\frac{\partial V_x}{\partial r}+\frac{1}{r}V_\theta\frac{\partial V_x}{\partial \theta}+V_x\frac{\partial V_x}{\partial x}\right)=-\frac{dP}{dx}+\rho g\sin\varnothing+\mu\left[\frac{1}{r}\frac{\partial}{\partial r}\left(r\frac{\partial V_x}{\partial r}\right)+\frac{1}{r^2}\frac{\partial^2 V_x}{\partial \theta^2}+\frac{\partial^2 V_x}{\partial x^2}\right] \tag{1}$$

where V_x, V_θ and V_r are the velocity components in the axial, azimuthal and radial directions, respectively; ρ is the density, and μ is the viscosity coefficient. The non-dimensional form of Eq. (1) is given by

$$\left(V_r^*\frac{\partial V_x^*}{\partial r^*}+\frac{1}{r^*}V_\theta^*\frac{\partial V_x^*}{\partial \theta}+V_x^*\frac{\partial V_x^*}{\partial x^*}\right)=-\frac{dP^*}{dx^*}+\frac{\sin\varnothing}{\mathrm{Fr}^2}+\frac{1}{\mathrm{Re}}\left[\frac{1}{r^*}\frac{\partial}{\partial r^*}\left(r^*\frac{\partial V_x^*}{\partial r^*}\right)+\frac{1}{(r^*)^2}\frac{\partial^2 V_x^*}{\partial \theta^2}+\frac{\partial^2 V_x^*}{\partial (x^*)^2}\right] \tag{2}$$

where non-dimensional variables are shown with an asterisk. In Eq. (2), velocities and spatial coordinate variables are nondimensionalized by the bulk (mean sectional) velocity V_b and channel radius R, respectively, whereas non-dimensional pressure $P^*=P/\rho V_\mathrm{b}^2$ is introduced as well. Re and Fr are the Reynolds and Froude numbers based on R and V_b ($\mathrm{Re}=\rho V_\mathrm{b}R/\mu$, $\mathrm{Fr}=V_\mathrm{b}/\sqrt{gR}$). The following simplifications can be made for uniform flow: (1) Flow is parallel to the wall everywhere and the only nonzero component of velocity is the axial velocity V_x^*, i.e., $V_r^*=V_\theta^*=0$; (2) axial derivative of the streamwise velocity is zero and thus the inertia term on the left-hand side and the last viscous term in the square bracket on the right-hand side of Eq. (2) vanish; (3) pressure is constant in the streamwise direction, i.e., $\mathrm{d}P^*/\mathrm{d}x^*=0$; (4) derivatives in the azimuthal coordinate (θ) direction are much smaller than those in the radial (r) direction and it is a reasonable approximation to neglect the second viscous term in Eq. (2). Validity of the last assumption is implicitly supported by the exact solution results given in Guo and Meroney [13] which show that constant velocity contours are almost parallel to each other and to the boundary of the circular channel wall for low-filled cases. The simplified form of Eq. (2) is then integrated twice in the radial direction between the wall ($r^*=1$) and the free surface ($r_s^*=r_s/R=(1-\frac{h}{R})/cos\theta$) to yield:

$$V_x^*(r^*,\theta)=-\frac{\mathrm{Re}}{4\mathrm{Fr}^2}\sin\varnothing(r^*)^2+C_1(\theta)\ln r^*+C_2(\theta) \tag{3}$$

where the integration constants $C_1(\theta)$ and $C_2(\theta)$ are evaluated by using the boundary conditions of (1) no-slip on the wall $V_x^*(1,\theta)=0$ and (2) zero velocity gradient in the r^* direction on the free surface $\left(\partial V_x^*/\partial r^*\right)_{r^*=r_s^*}=0$. The proper boundary condition used in the exact solution of Guo and Meroney [13] is $\partial V_x/\partial y=0$ on the free surface. This zero shear stress boundary condition assumes that the gas above the liquid has negligibly small viscosity. The continuity equation is satisfied by our approximate solution since the only nonzero velocity component V_x^* does not depend on the streamwise coordinate in uniform flow. Solution of the dimensionless momentum equation (i.e., Eq. 3) is given by:

$$V_x^*=\frac{Re}{4\mathrm{Fr}^2}\sin\varnothing\left[1-(r^*)^2+\frac{2}{\cos^2\theta}\left(1-\frac{h}{R}\right)^2\ln r^*\right] \tag{4}$$

Guo and Meroney [13] define a new dimensionless velocity U, given by $U=V_x^*\frac{\mathrm{Fr}^2}{\mathrm{Re}\sin\varnothing}=\mu V_x/\left(R^2\rho g\sin\varnothing\right)$ which is written explicitly as

$$U=\frac{1}{4}\left[1-(r^*)^2+\frac{2}{\cos^2\theta}\left(1-\frac{h}{R}\right)^2\ln r^*\right] \tag{5}$$

Equations (4) and (5) are valid only for low-filled case where the depth ratio h/R is smaller than one. The normalized wall shear stress (friction factor) is defined as $T_0=-\mu\left(\partial V_x/\partial r\right)/\rho gR\sin\varnothing$ and for the approximate solution is given by

$$T_0=\frac{1}{2}\left[1-\left(1-\frac{h}{R}\right)^2\frac{1}{cos^2\theta}\right] \tag{6}$$

The dimensionless centerline surface velocity U_o (at $r=R-h$ and $\theta=0$) is given by

$$U_0=\frac{1}{4}\left[\frac{h}{R}\left(2-\frac{h}{R}\right)+2\left(1-\frac{h}{R}\right)^2\ln\left(1-\frac{h}{R}\right)\right] \tag{7}$$

The bulk (mean sectional) velocity V_b is defined by

$$V_\mathrm{b}=\frac{\iint V_x r\mathrm{d}r\mathrm{d}\theta}{A} \tag{8}$$

where integration is carried out from $-\varphi$ to φ for θ and from r_s to R for r. φ is the maximum value of θ given by $\varphi=\cos^{-1}(1-h/R)$ (See Fig. 1) and A is the cross-sectional flow area given by $A=R^2(\varphi-\sin\varphi\cos\varphi)$. The integral in Eq. (8) is evaluated analytically producing the following

expression for the approximate normalized bulk velocity ($U_b = \mu V_b/\left(R^2\rho g\sin\varnothing\right)$):

$$U_b = \frac{1}{4(\varphi - \sin\varphi\cos\varphi)}\left[\frac{\varphi}{2} - 2\left(1-\frac{h}{R}\right)^2\tan\varphi + \frac{1}{6}\left(1-\frac{h}{R}\right)^4(\cos(2\varphi)+2)\frac{\tan\varphi}{\cos^2\varphi}\left(3+4\ln\frac{R\cos\varphi}{R-h}\right)\right] + \frac{1}{9}\left(1-\frac{h}{R}\right)^4\left(2\frac{\tan\varphi}{\cos^2\varphi}+10\tan\varphi-12\varphi\right) \tag{9}$$

The momentum flux and kinetic energy flux correction factors (β and α) are defined, respectively, by:

$$\beta = \frac{\iint V_x^{\,2} r\mathrm{d}r\mathrm{d}\theta}{AV_b^{\,2}} \tag{10}$$

$$\alpha = \frac{\iint V_x^{\,3} r\mathrm{d}r\mathrm{d}\theta}{AV_{\mathrm{b}}^{\,3}} \tag{11}$$

β and α are the correction factors used in calculating momentum and kinetic energy fluxes, respectively, in engineering applications. The correction factors are the ratio of real fluxes to the idealized fluxes calculated by assuming uniform velocity in cross section of flow. The integrals in Eqs. (10) and (11) are evaluated numerically (from $-\varphi$ to φ for θ and from r_s to R for r) and variations of β and α with h/R (including some algebraic expressions) are presented in the next section. A relationship between the correction factors for momentum and energy fluxes is established and compared with data reported in the literature.

3 Results

3.1 Velocity contours and profiles

Figure 2a, b give a comparison of the normalized streamwise velocity U contour plots predicted by the approximate (present study) and exact [13] solutions, respectively, for the depth ratio (h/R) of 0.5. The channel wall is indicated by a thick circular line. Contours of both solutions are normal to the $z/R = 0$ centerline due to flow symmetry. The overall agreement between the solutions is rather good, especially near the channel wall. Disagreement between the contours is readily observable near the free surface where contours are inclined with respect to the free surface for the approximate solution (Fig. 2a), while they are normal to the surface for the exact solution (Fig. 2b). The boundary condition employed in the approximate solution forces the contours to turn inwards such that tangents to the contours on the free surface pass through the origin of the coordinate system. Thus, for the exact solution, the free surface is a virtual plane of symmetry, whereas for the approximate solution the virtual plane of symmetry rotates slightly. Experimentally obtained velocity contour plots reported in [15–17] also show an inclination of contours like that in Fig. 2a. This behavior of velocity contours is due to secondary flows generated by turbulence [17] or nonuniformity of flow (nonzero inertia terms in the axial momentum equation).

Figure 3 presents variation of the normalized streamwise velocity (U) with the normalized vertical distance measured from the channel surface (y_s/R), on the centerline ($z/R = 0$) for $h/R = 0.3$, 0.6 and 0.9. The filled symbols connected by a curve denote the exact solution of Guo and Meroney [13]. It can be observed from Fig. 1 that y_s and y are related by $y_s = y_w - \mathrm{y}$ where y_w is the y coordinate of the circular channel wall. The maximum value of y_s/R is located on the free surface. The side-view velocity profiles given by Fig. 3 show that on the symmetry plane ($z/R = 0$), the velocity predicted by the approximate solution (and hence the centerline velocity on the free surface, U_0) is always higher than that of the exact equation.

Figure 4a, b present variations of the normalized streamwise velocity (U) with the normalized vertical distance measured from the channel surface (y_s/R) along three vertical lines ($z/R = 0.20$, 0.40 and 0.60) and with the normalized spanwise distance (z/R) along three horizontal lines ($y/R = 0.6$, 0.75 and 0.90) for $h/R = 0.5$, respectively. The filled symbols connected by a curve denote the exact solution of Guo and Meroney [13]. Figure 4a shows that velocity predicted by the approximate solution is smaller and larger than those of the exact solution near the centerline ($z/R = 0.2$) and near the channel edge ($z/R = 0.6$), respectively. In all profiles, agreement between the two solutions is good near the channel wall (small y_s/R) where both solutions use the same (no-slip) boundary condition. The top-view velocity profiles in Fig. 4b show that velocity is overpredicted by the approximate solution near the channel wall ($y/R = 0.75$ and 0.90). Near the free surface ($y/R = 0.6$), approximate solution has high bias near the centerline and low bias near the channel edge. Differences between the approximate and exact solutions remain smaller than 15% of the centerline velocity.

Figure 5a, b present variations with the depth ratio (h/R) of a) normalized bulk velocity (U_b), b) ratio of bulk velocity to the centerline surface velocity (U_b/U_o), respectively, for the approximate and exact solutions. Equations (7) and (9) are used to plot the data of the approximate solution. Figure 5a shows that U_{b} normalized bulk velocity values predicted by the approximate solution are slightly larger than those of the exact solution. On the other hand, as shown in Fig. 5b, $U_{\mathrm{b}}/U_{\mathrm{o}}$ values of the approximate solution are smaller than those of the exact solution. This is due to the over-prediction of the centerline surface velocity U_o by

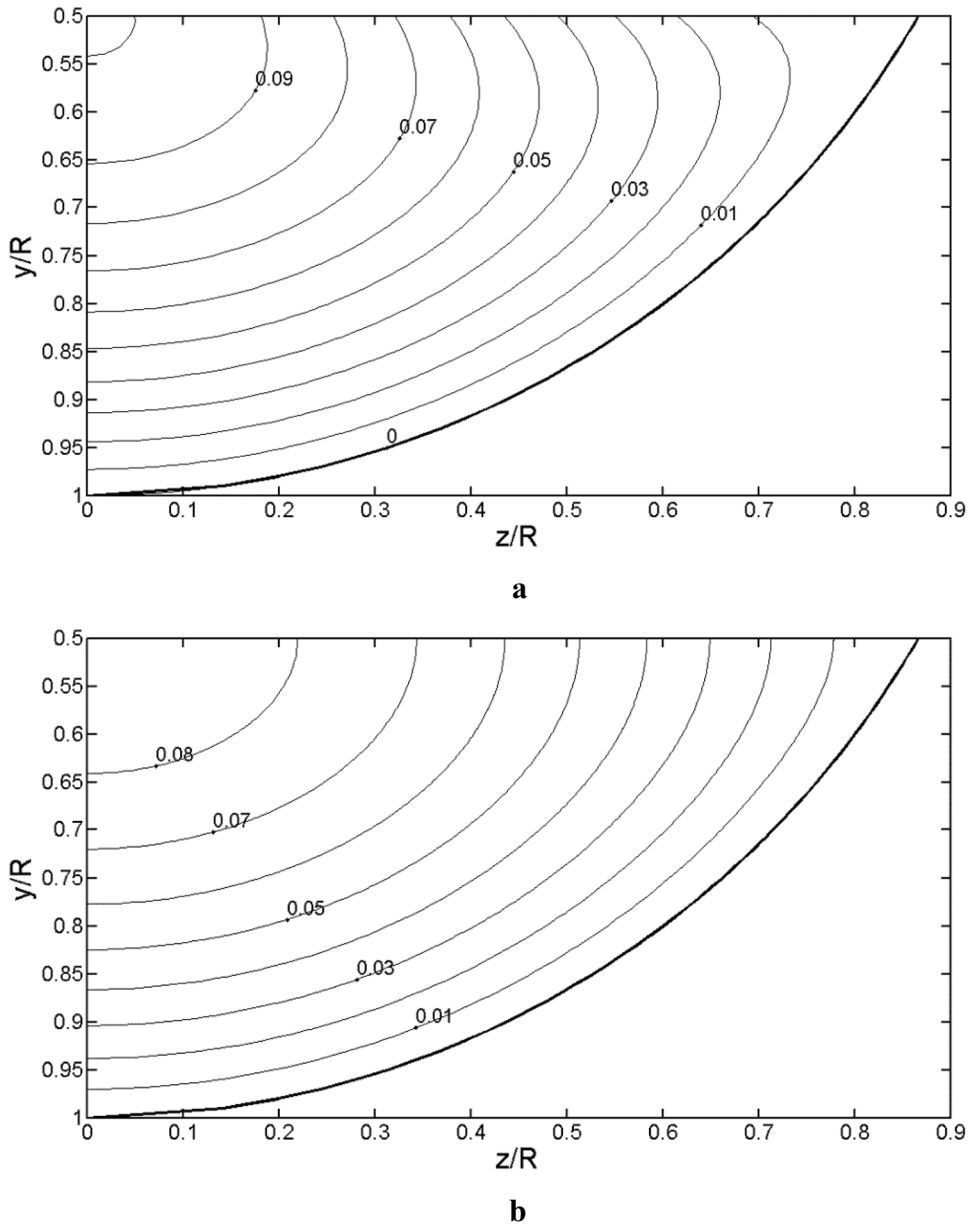

Fig. 2 Normalized streamwise velocity (U) contour plots for h/R value of 0.5 **a** approximate solution and **b** exact solution [13]

the approximate solution. As noted by Fullard and Wake [14] for laminar flow, U_o remains the maximum velocity in the flow field up to the h/R value of 0.86 above which location of the velocity maximum moves below the surface (velocity dip phenomena). A third-order polynomial curve fit to the exact solution of Guo and Meroney [13] gives the following expression for the variation of U_b with h/R:

$$U_{\mathrm{b}} = 0.003\left(\frac{h}{R}\right) + 0.211\left(\frac{h}{R}\right)^2 - 0.089\left(\frac{h}{R}\right)^3 \tag{12}$$

which is also plotted in Fig. 5a. A second-order polynomial curve fit to the exact solution of Guo and Meroney [13] produces the following expression for $U_{\mathrm{b}}/U_{\mathrm{o}}$:

$$\frac{U_{\mathrm{b}}}{U_0} = 0.461 + 0.098\left(\frac{h}{R}\right) - 0.062\left(\frac{h}{R}\right)^2 \tag{13}$$

which is plotted in Fig. 5b and represents the exact solution with a relative error of 0.5%.

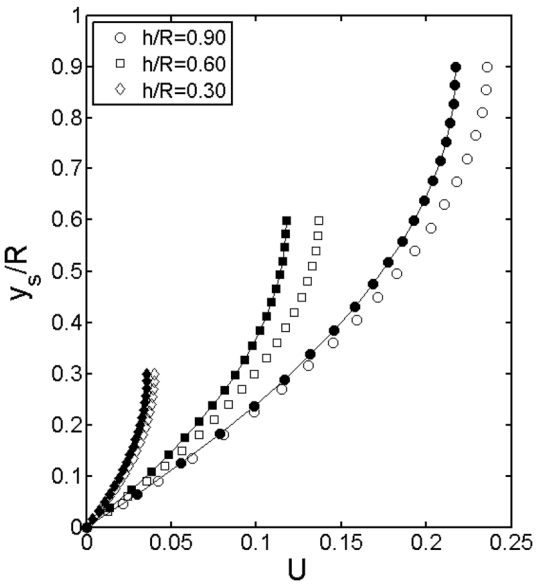

Fig. 3 Variation of streamwise velocity (U) with y_s/R on the centerline (z/R=0) for h/R=0.3, 0.6 and 0.9

3.2 Surface shear stress

Figure 6 presents variation of the normalized wall shear stress T_o with the azimuthal coordinate θ for h/R=0.3, 0.6 and 0.9; calculated using Eq. (6). T_o variations predicted by the exact solution of Guo and Meroney [13] are also presented (filled symbols connected by a curve). Comparison of the approximate and exact variations shows reasonably good agreement. Good agreement of wall shear stress is expected because of the small magnitude of velocity errors near the channel wall.

3.3 Correction factors for momentum and kinetic energy flux

Figure 7a, b present variations of the correction factors for momentum flux (β) and kinetic energy flux (α), respectively. Variations predicted by the exact solution of Guo and Meroney [13] and linear curve fits to the exact solution are also presented in Fig. 7. Comparison of the approximate and exact variations shows reasonably good agreement. Both solutions give the same values of β=1.33 and α=2.0 for h/R=1 (which are identical to the correction factor values for laminar pressurized pipe flow). Figure 7a, b show that β and α values predicted by the approximate solution are consistently higher than those of the exact solution. Discrepancies between the approximate and exact values of β and α are largest around h/R values of 0.5. This is expected because U_b/U_o ratio also has a similar trend as shown in Fig. 5b. Discrepancies between the approximate and exact solutions are less than 5% for β and 10% for α. A larger discrepancy for α is expected because of the third power of V_x/V_b in the definition of α (Eq. 11), instead of the second power in the definition of β (Eq. 10), and subsequent propagation of errors. The second-order polynomial curve fits to the exact solution of Guo and Meroney [13] produce:

$$\beta = 1.40 - 0.17\left(\frac{h}{R}\right) + 0.10\left(\frac{h}{R}\right)^2 \tag{14}$$

$$\alpha = 2.23 - 0.58\left(\frac{h}{R}\right) + 0.36\left(\frac{h}{R}\right)^2 \tag{15}$$

which are also shown in Fig. 7 and represent the exact solution within relative uncertainty levels of 1%.

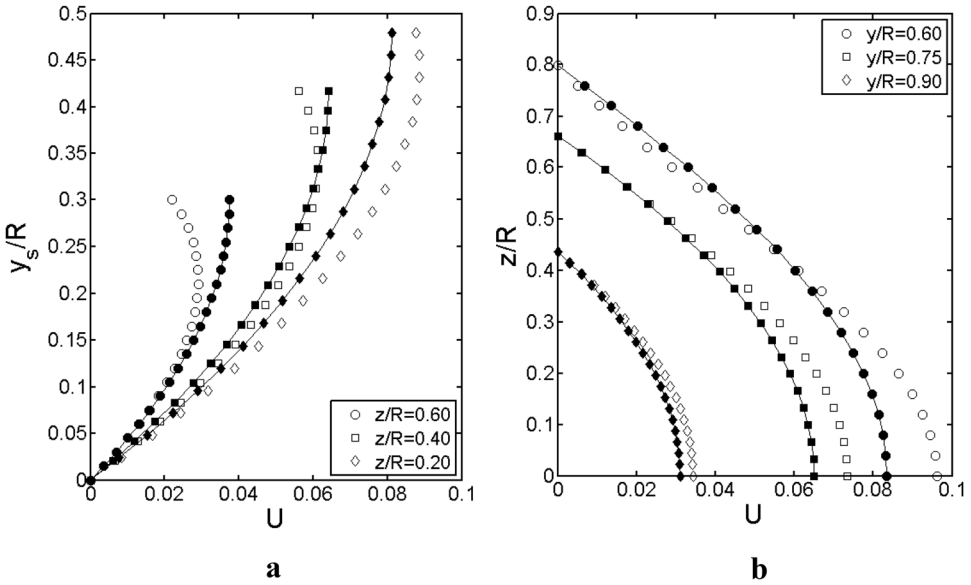

Fig. 4 Variation of streamwise velocity (U) for h/R=0.5 **a** with y_s/R at z/R=0.20, 0.40 and 0.60, **b** with z/R at y/R=0.6, 0.75 and 0.90

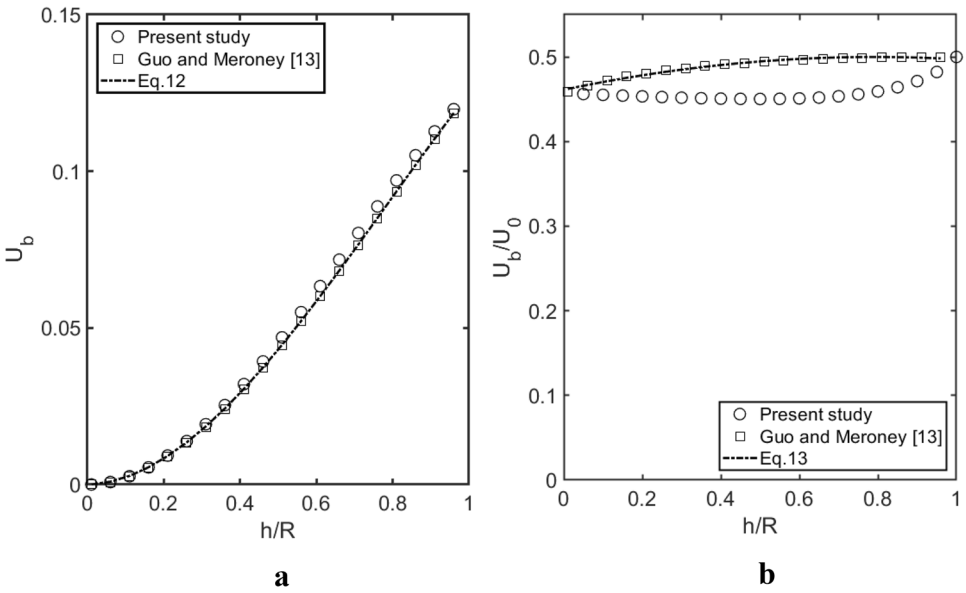

Fig. 5 Variation of **a** normalized bulk velocity (U_b) and **b** ratio of bulk velocity to centerline surface velocity (U_b/U_o) with the depth ratio (h/R)

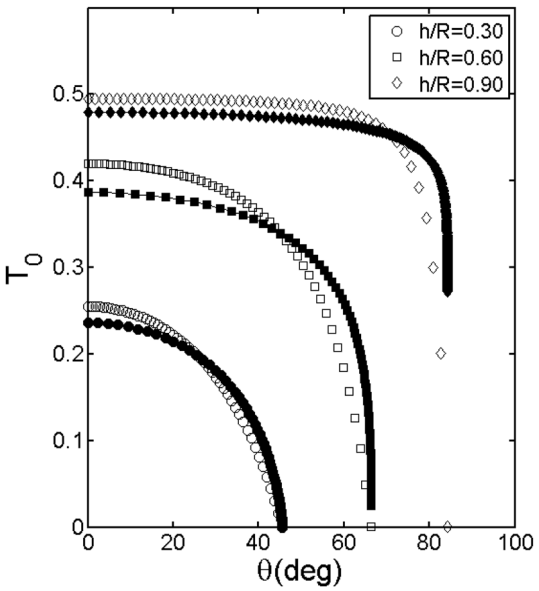

Fig. 6 Variation of the normalized wall shear stress T_o with the azimuthal coordinate θ for $h/R = 0.3$, 0.6 and 0.9

Figure 8 shows the relationship between the correction factors for kinetic energy flux (α) and momentum flux (β) for all values of h/R considered in the previous figures. The data of Guo and Meroney [13] can be represented by a linear fit given below (Eq. (16)) with an accuracy better than 99.9%.

$$\alpha = 3.48\beta - 2.64 \quad \text{for} \quad 1.33 < \beta < 1.40 \tag{16}$$

Equation (16) is valid for laminar flow in a smooth circular channel. For turbulent flow, large scale mixing provides better flow uniformity compared to laminar flow and produces lower values of the correction factors. For example, Chow [15] reports that the average approximate values of α and β are 1.15 and 1.05, respectively, for regular channels. For turbulent flow in compound channels, much larger values of α and β are revealed by the experimentally obtained correlations of Mohanty et al. [18] which are plotted in Fig. 8 for comparison. Chiu and Tung [19] propose algebraic relations for variations of α and β in terms of a probability distribution parameter. Figure 8 also shows the data of Chiu and Tung [19] which is in very good agreement with Eq. (16). The correlations of Mohanty et al. [18] and Chiu and Tung [19] extend to lower values of the coefficients and originate from $\alpha = \beta = 1$

4 Concluding remarks

Solutions to the laminar free-surface flow reported previously in the literature mostly require numerical evaluation of integral terms, which are not suitable for daily engineering practice. In the present study, an approximate analytic solution of laminar flow in a circular open channel is presented by employing some simplifications. Neglect of the second-order velocity derivatives in the azimuthal direction, and velocity gradient in the radial direction at the free surface allows a pure analytical solution of the steady incompressible Navier–Stokes equations in cylindrical coordinates. Accuracy of the approximate solution is assessed by comparison with the exact theoretical solution of Guo and Meroney [13]. In contrast to the solutions of Guo and Meroney [13] and Fullard and Wake [14] that require numerical evaluation, the approximate solution has a quite simple form and

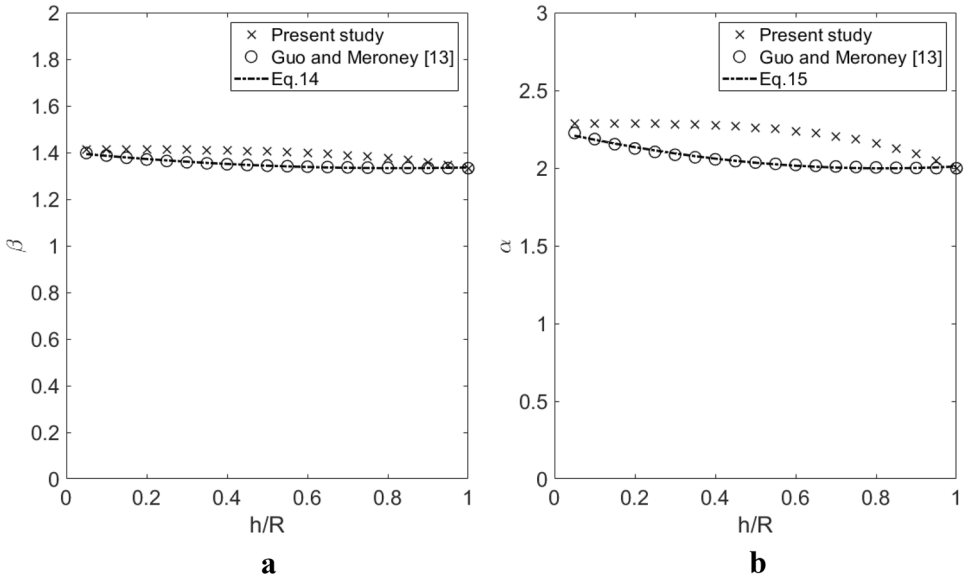

Fig. 7 Variations with the depth ratio (h/R) of correction factors for **a** momentum flux (β), and **b** kinetic energy flux (α)

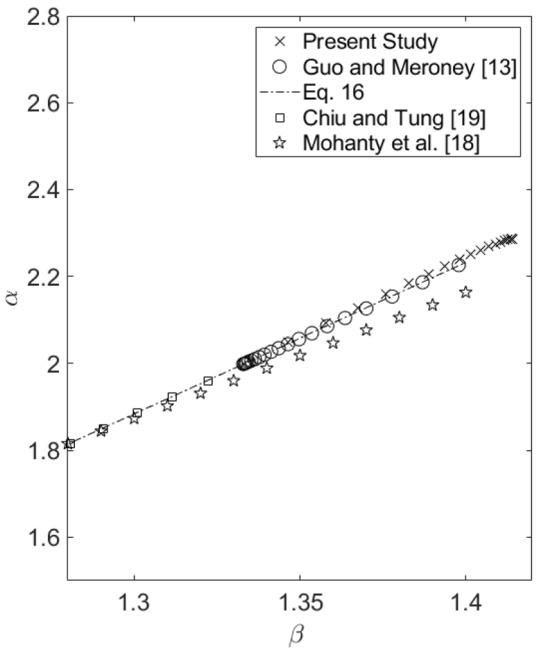

Fig. 8 Relationship between the kinetic energy correction factor (α) and momentum correction factor (β)

agrees reasonably well with the exact solution. The good agreement between the approximate and exact solutions verifies that the assumptions employed in the derivation of the approximate solution are realistic from an engineering point of view. Based on the approximate solution, algebraic expressions for the cross-sectional distribution of velocity and wall shear stress, as well as variation of momentum and kinetic energy correction factors with flow depth, are presented. A relationship between the momentum and energy correction factors is established and compared with data reported in the literature.

References

1. Berker R (1963) Integration des equations du movement d'un fluide visqueux incompressible. In: Flugge (ed) Handbuch der Physik, vol VIII/2. Springer, Berlin
2. Wang CY (1989) Exact solutions of unsteady Navier-Stokes Equations. Appl Mech Rev 42(11S):S269–S282
3. Berker R (1982) An exact solution of the Navier-Stokes equation. Int J Eng Sci 20(2):217–230
4. Rajagopal KR (1984) A class of exact solutions to the Navier-Stokes equations. Int J Eng Sci 22(4):451–458
5. Terrill RM, Colgan T (1991) Some simple analytical solutions of the Navier-Stokes equations. Int J Eng Sci 29(1):55–68
6. White F (2015) Fluid mechanics, 8th edn. McGraw-Hill, New York
7. O'Brien V (1977) Steady and unsteady flow in noncircular straight ducts. J Appl Mech 44(1):1–6
8. McKerrell A (1988) The global element method applied to fluid flow problems. Comput Fluids 16(1):41–46
9. Duck PW (1979) Flow in straight ducts of arbitrary cross section. J Appl Mech 46(2):263–268
10. Mazumdar J, Dubey RN (1991) A method for the study of fully developed parallel flow in straight ducts of arbitrary cross section. ANZIAM J 33(2):211–239
11. Sari MR, Kezzar M, Adjabi R (2014) A comparison of Adomian and Generalized Adomian Methods in solving the nonlinear problem of flow in convergent-divergent channels. Appl Math Sci 8(7):321–336
12. Kezzar M, Sari MR (2015) Application of the generalized decomposition method for solving the nonlinear problem of Jeffery-Hamel flow. Comput Math Model 26(2):284–297
13. Guo J, Meroney RN (2013) Theoretical solution for laminar flow in partially-filled pipes. J Hydraul Res 51(4):408–416
14. Fullard LA, Wake GC (2015) An analytical series solution to the steady laminar flow of a Newtonian fluid in a partially filled pipe including the velocity distribution. IMA J Appl Math 80(6):1890–1901
15. Chow VT (1959) Open channel hydraulics. McGraw-Hill, New York
16. Yoon J, Sung J, Lee MH (2012) Velocity profiles and friction coefficients in circular open channels. J Hydraul Res 50(3):304–311

17. Knight DW, Sterling M (2000) Boundary shear in circular pipes running partially full. J Hydraul Eng 126(4):263–275
18. Mohanty PK, Dash SS, Khatua KK, Patra KC (2013) Energy and momentum coefficients for wide compound channels. WIT Trans Ecol Environ 72:87–97
19. Chiu CL, Tung NC (2002) Maximum velocity and regularities in open-channel flow. J Hydraul Eng 128(4):390–398